UPPSALA
UNIVERSITET

Digital Comprehensive Summaries of Uppsala Dissertations from the Faculty of Science and Technology 802

Measurements of Angular Correlations in Minimum Bias Events and Preparatory Studies for Charged Higgs Boson Searches at the Tevatron and the LHC

CAMILLE BÉLANGER-CHAMPAGNE

ACTA
UNIVERSITATIS
UPSALIENSIS
UPPSALA
2011

ISSN 1651-6214
ISBN 978-91-554-7989-3
urn:nbn:se:uu:diva-142464

Dissertation presented at Uppsala University to be publicly examined in Polhemsalen, Ångströmlaboratoriet, Lägerhyddsvägen 1, Uppsala, Friday, March 4, 2011 at 13:15 for the degree of Doctor of Philosophy. The examination will be conducted in English.

Abstract

Bélanger-Champagne, C. 2011. Measurements of Angular Correlations in Minimum Bias Events and Preparatory Studies for Charged Higgs Boson Searches at the Tevatron and the LHC. Acta Universitatis Upsaliensis. *Digital Comprehensive Summaries of Uppsala Dissertations from the Faculty of Science and Technology* 802. 50 pp. Uppsala.
ISBN 978-91-554-7989-3.

Studies of minimum bias events at colliders probe the behavior of QCD in the non-perturbative regime. The phenomenology of events in this regime is described by empirical models that take many parameters, which all need to be tuned to the observed data. Measurements based on angular correlations between the highest transverse momentum charged particle track and the other charged particle tracks in collision events can, because of their robustness against experimental and detector effects, be a component of the tuning inputs for the models. We measure such observables in a variety of pseudorapidity ranges and at many center-of-mass energies at DØ and ATLAS. We observe that such observables are poorly described by current models and tunes that are used to produce simulated event samples, making them valuable information for the tuning process.

The Matrix Element method is a powerful analysis tool to extract precise measurements from data samples of limited statistics. We have investigated the potential of the Matrix Element method to measure the mass of the charged Higgs in the exclusive decay $H^{\pm}\rightarrow\tau^{\pm}\nu\rightarrow e^{\pm}+3\nu$ when produced in top quark decays at the Tevatron, with emphasis on the construction of transfer functions in the τ decay chain. We concluded that the τ decay chain can be successfully parametrized via a transfer function and that the method has the potential to provide an accurate charged Higgs mass measurement in this channel.

Triggering on τ leptons is a key component for many beyond the Standard Model searches at ATLAS, such as the search for the charged Higgs boson. Events containing Z bosons can be used to measure the efficiency of the ATLAS τ hadronic-decay trigger. We have used a tag-and-probe method on simulated Z boson decays to 2 τ leptons where one decays to a μ while the other decays hadronically. The μ is used as the tag and the τ side is probed. We demonstrated that the efficiency of the τ hadronic-decay trigger can be accurately measured with this method using the first 100 pb^{-1} of ATLAS data.

Keywords: ATLAS, D0, LHC, Tevatron, CERN, Fermilab, QCD, Monte Carlo tunes, Matrix Element method, Charged Higgs boson, Tau lepton, Trigger

Camille Bélanger-Champagne, Department of Physics and Astronomy, High Energy Physics, 516, Uppsala University, SE-751 20 Uppsala, Sweden.

ISSN 1651-6214
ISBN 978-91-554-7989-3
urn:nbn:se:uu:diva-142464 (http://urn.kb.se/resolve?urn=urn:nbn:se:uu:diva-142464)

List of Papers

This thesis is based on the following papers, which are referred to in the text by their Roman numerals.

I DØ Collaboration
Study of ϕ and η correlations in minimum bias events with the DØ detector at the Fermilab Tevatron collider
DØ Note 6054-CONF (2010)

II ATLAS Collaboration
Angular correlations between charged particles from proton-proton collisions at $\sqrt{s}$ = 900 GeV and $\sqrt{s}$ = 7 TeV measured with the ATLAS detector
ATLAS-CONF-2010-082 (2010)

III Bélanger-Champagne, C., Buszello, C., Ekelöf, E.
Transfer function treatment of leptonic τ decays in the Matrix Element method
PoS(CHARGED2010) 006 (2011)

IV Brenner, R. *et al*.
The ATLAS tau trigger and planned trigger efficiency studies with early data
PoS(CHARGED2008) 027 (2009)

Complementary papers not included in this thesis:

- Bélanger-Champagne, C. for the ATLAS Collaboration
  Study of charged particle correlations and underlying events with the ATLAS detector
  ATL-PHYS-PROC-2010-146 (2010)
  Submitted to the Proceedings of WPCF 2010

- Casado, M. P. *et al*.
  The ATLAS tau trigger
  ATL-DAQ-PROC-2008-008, ATL-COM-DAQ-2008-017
  Nucl. Phys. B, Proc. Suppl. 189 (2009)

Contents

1. Introduction

Particle physics has the broad-reaching goal of describing the building blocks of all the matter in our Universe and the forces that define their behavior. The research field known as high energy physics utilizes collisions at the highest achievable energies to expand our knowledge at the so-called "energy frontier", that is at hitherto unprobed energy densities were new phenomena are most likely to be discovered. This links the field to that of cosmology, since higher energy densities are akin to the early universe. The Standard Model of particle physics describes the current status of knowledge on these topics. This scientific theory is one of the most successful scientific achievements of the 20^{th} century. The theory has produced many testable predictions that have turned out to be fulfilled in experiments, and its accuracy has been found to be remarkable.

However, precision measurements of the Standard Model are still ongoing as there are areas of the Standard Model where the current experimental precision is not enough to rule out phenomena that are not described by the Standard Model. Furthermore, physics phenomena have been observed that cannot be explained by the Standard Model, indicating that its current content will, at least, require some extensions. Among the best known such phenomena are the existence of dark matter and dark energy in the Universe as well as the insufficient amount of charge-parity violation in the model to account for the matter-antimatter asymmetry of the Universe.

Particle physics laboratories are at the heart of the global scientific effort to understand the basic structure of the Universe. High-energy particle collisions are created in particle accelerators at energies that have never before been available in laboratory settings. The Tevatron collider at Fermilab and the Large Hadron Collider at the CERN laboratory are home to large experimental collaborations that build detectors to reconstruct and understand the results of these collisions. Some results from two such large collaborations, DØ at Fermilab and ATLAS at CERN are presented in the papers included in this thesis.

To put the content of these papers in context, some general background information will be presented. This information is provided in the first part of this thesis. In Chapter 2, some theoretical background to the Standard Model is provided, emphasizing the Quantum Chromodynamics theory, which describes the strong nuclear interaction. Extensions to the Standard Model Higgs sector that result in the existence of a charged Higgs boson are also presented.

In Chapter 3, we describe the experimental apparatuses that were used to produce the results presented in the papers: the Tevatron accelerator with the DØ detector and the LHC accelerator with the ATLAS detector. In Chapter 4, we introduce in some detail the Matrix Element method, a multivariate analysis method used in Paper III.

After this background is set in place, we summarize the content of each paper in Chapter 5. In Chapter 6 we provide a summary of the thesis in Swedish.

2. The Standard Model and beyond

In this chapter, the Standard Model of high energy physics is presented. Special emphasis is put on Quantum Chromodynamics in the non-perturbative regime and on the Higgs sector, which are especially relevant to the studies presented in this thesis.

2.1 Standard Model

The Standard Model is a relativistic quantum field theory that describes the particles that make up matter and their interactions through three of the four fundamental forces of nature: the electromagnetic force, the weak force and the strong force. The fourth fundamental force is gravity. Gravity is currently best described in the geometric framework of general relativity and as such is not described within the relativistic quantum field theory framework of the Standard Model. In the Standard Model, particles with spin $1/2$, called fermions, come in two types according to their interactions and their electric charge. Leptons can interact through the electro-weak force and have integer electric charges. Quarks interact through the electro-weak force as well as through the strong force and have fractional electric charges. Matter particles can be further classified in three generations that can transform into each other via the weak force. The first generation is composed of particles that make up most of the matter around us: the up and down quarks, the lepton called the electron and its associated neutrino. The particles of the other generations share most of the properties of the first generation particles but have higher masses and are not stable: they rapidly decay to their lighter, stable counterparts. The main properties of the Standard Model fermions are listed in Table 2.1.

Each matter particle has an equivalent anti-matter particle. Anti-matter particles have the same mass, spin and interactions as their matter counterparts but opposite electrical charges. Some of their quantum numbers are also opposite to those of the corresponding matter particles, for example their lepton number is chosen to be different.

Interactions in the Standard Model are mediated through spin 1 particles called bosons. Photons mediate electromagnetic interactions, Z^0, W^+ and W^- bosons are carriers of the weak force and gluons mediate the strong interaction. The strength of each type of interaction is related to the interaction cou-

pling associated with each force. Table 2.2 lists the main properties of the Standard Model bosons. For a more complete review of the Standard Model, see References [1, 2].

	Lepton	Charge	Mass (MeV)	Quark	Charge	Mass (MeV)
I	e	-1	0.511	u	+2/3	1.7-3.3
	ν_e	0	$< 2 \times 10^{-6}$	d	-1/3	4.1-5.8
II	μ	-1	105.7	c	+2/3	1.18-1.34 $\times 10^3$
	ν_μ	0	< 0.19	s	-1/3	80-130
III	τ	-1	1776.8	t	+2/3	172 $\times 10^3$
	ν_τ	0	< 18.2	b	-1/3	4.1-4.4 $\times 10^3$

Table 2.1: *Properties (electric charge and mass) of Standard Model fermions. The roman numerals indicate the three generations of fermions.*

Force	Boson	Charge	Mass (GeV)
Electromagnetic	γ	0	0
Weak	Z^0	0	91.19
	$W^\pm$	± 1	80.40
Strong	g	0	0

Table 2.2: *Properties (electric charge and mass) of Standard Model gauge bosons.*

2.2 QCD and the non-perturbative regime

Quantum Chromodynamics (QCD) is the name given to the relativistic quantum field theory that describes strong force interactions within the Standard Model. It describes interactions between quarks and gluons. For a more complete review of QCD, see References [1, 3, 4]. The quark model associates a quantum number called color to quarks and gluons. The color quantum number can take the values red, green or blue or the associated anti-colors for quarks and gluons whereas it is zero for other particles in the Standard Model. Quarks carry one color while gluons carry a mix of two colors. As carriers of the strong force, gluons interact with particles that have non-zero color charge. Gluons couple to quarks as well as other gluons since they also carry a non-zero color charge.

Unlike other forces in the Standard Model for which the value of the coupling strength rises with decreasing interaction distance, the value of the strong coupling strength α_s decreases with decreasing interaction distance. This property of the strong force is called *asymptotic freedom*. It makes the strong force a confining force that increases with distance for particles that have a net color charge. The strength of the coupling α_s is also important when it comes to doing calculations within QCD. The coupling α_s enters into QCD calculations for each interaction "vertex" between quarks and gluons. A physical process can be described as the sum of an infinite series of component processes with increasing number of vertices, giving successive terms in the series proportional to α_s^n for increasing power n. By truncating the series after the leading order term, the next-to-leading order term and so forth, successive approximations are obtained at different accuracy levels. This perturbation theory breaks down if α_s becomes too large in processes with low momentum transfer, giving rise to a non-perturbative regime of QCD.

In the framework of QCD, states that do not have an overall color charge of zero are forbidden by the color confinement principle and only color-singlet states are allowed. Bound states of two quarks are called mesons while bound states of three quarks are called baryons.

The existence of isolated quarks is forbidden by QCD coupling behavior. Whenever a particle collision produces an isolated quark or gluon, the particle will undergo a process called hadronization where a cascade of quark-antiquark pairs is created from the energy in the color force field in order to form bound states as required by color confinement. The macroscopic result of hadronization is the production of a jet of hadrons. A few theoretical models [3] exist that attempt to describe the hadronization process. The increase in the complexity of QCD models of jet formation is approximately factorial with each order in perturbative calculations. Models also contain a regime where non-perturbative effects dominate and where the tools of perturbation theory cannot be used in calculations. The energy limit where transition to the non-perturbative regime happens is a parameter of the model and is usually tuned to give the best agreement to data.

2.2.1 Minimum bias collisions and the underlying event

To study the phenomenology of non-perturbative QCD in experimental data, event samples are constructed were these effects dominate. The underlying event in hard scattering processes has been investigated in this way. The underlying event (UE) is the name given to all the soft interactions that occur in a particle collision, except for the hardest scattering process. It includes initial and final state radiation, which cannot be distinguished from the UE. A schematic representation of a hard scattering process and its UE is shown in Figure 2.1. The hard scattering processes that are most often used in UE

studies are Drell-Yan events, and events in which a pair of energetic jets are produced [5]. To create a region where the UE properties dominate, each event is rotated, in the transverse plane of the detector, so that its component with the highest transverse momentum is located at azimuthal angle $\phi = 0$. The azimuthal region $60^{o} < \Delta\phi < 120^{o}$ is then orthogonal to the axis of the hard scattering and thus most representative of the properties of the UE. Kinematic distributions such as the charged particle density and mean transverse momentum are measured in this region and constitute an experimental description of the UE.

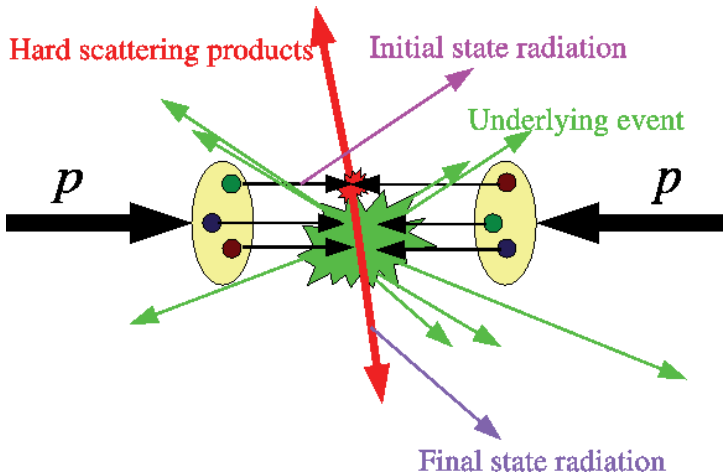

Figure 2.1: Schematic representation of the components of the underlying event of a hard scattering collision.

Non-perturbative QCD phenomenology can also be studied in minimum bias event samples. These event samples are selected so they present as small as possible of a trigger bias in the data acquisition, and thus are as representative as possible of the overall collision cross-section at colliders [6]. Minimum bias samples are mostly comprised of QCD single gluon-gluon or quark-quark elastic scattering events and single and double diffraction events. The phenomenology of these events as a whole is dominated by non-perturbative QCD effects. Many methods exist to select minimum bias event samples. Most often, dedicated trigger systems are used, as is the case in the study presented in Paper II. It is also possible to take advantage of the naturally occurring overlap of collisions in the detector, called pile-up, to construct the samples, as is the case in the study presented in Paper I.

2.2.2 Monte Carlo tuning

Collisions simulated in Monte Carlo (MC) event generators aim to reproduce both the observed non-perturbative behavior of QCD and the higher trans-

verse momentum transfer behavior where perturbation theory can be used to make accurate calculations. To describe the behavior in the kinematic region where perturbation theory cannot be used, empirical models have been developed. Such models exist not only for the partonic level of the UE, but also for the parton distribution functions in the hadrons, the initial and final state radiation, the hadronization process, the behavior of the beam remnants and the color reconnection process. These models rely on a large number of parameters that need to be carefully adjusted to provide the best match to a set of experimental measurements. Many of the parameters have physical meaning within their model and their values are expected to fall within a predicted range, even if the exact value cannot be predicted by the theory. The collection of a set of models that cover all components of a collision and the parameter values for these models that have been adjusted such that the model description fits best the experimental data is called a "tune", in reference to the process of fitting the model to experimental data. While some aspects of the phenomenology depend more on certain model components or certain parameters, a tune is a complex, interdependent system and in general a complete retuning is necessary for any change made to a single component. The studies presented in Papers I and II demonstrate that some components of the tunes available in the event generator PYTHIA [7] have a greater effect on angular correlations than others. This is valid, in particular, for the choice of shower model, the use of a color reconnection model and the relative contribution of hard and soft components to the description of the phenomenology. The evolution of partonic showers in collision events can be calculated using a virtuality-ordered or a transverse momentum-ordered mechanism. The tunes by Rick Field such as Tune A and Tune DW use virtuality-ordered showers while the Perugia tunes [8] such as P0, PHARD and PSOFT all use transverse momentum-ordered showers. Those family of tunes produce vastly different predictions of angular correlations in minimum bias events, and are compared to measured data distributions in Papers I and II. In general, tunes using transverse momentum ordered showers provide a qualitatively better match to the data.

It is possible to construct tunes where, during the tuning process, one tries to model as much as possible of the phenomenology via the hard or the soft components, respectively. PHARD and PSOFT are two such cases, where the hard and soft components, respectively, are enhanced relative to the more balanced tune P0. They affect the prediction of angular correlations and it is PHARD that produces the prediction that, while not a perfect fit to the data, is qualitatively best overall.

Finally, color reconnection models work in the framework of the Lund string model to allow reconfiguration of the color string layout. The effect of the change of the color reconnection model is smallest among those highlighted here but allowing color reconnections in the Lund string model tends to improve the description of the data.

2.3 Mass and the Higgs sector

There is one more boson in the Standard Model than those listed in Table 2.2. It is the Higgs boson, the only Standard Model particle that has not yet been observed. The Higgs boson arises from the Higgs field which is a complex scalar field doublet with four degrees of freedom. The Higgs field gives mass to the $W^{\pm}$ and Z^0 bosons through spontaneous symmetry breaking via the Higgs mechanism, consuming three of the four degrees of freedom, and to fermions via Yukawa couplings between the fermions and the Higgs field. These masses could not arise via explicit mass terms in the Lagrangian, because such terms would not be gauge-invariant. The remaining degree of freedom gives rise to a physical particle, the Higgs boson. The Higgs boson is electrically neutral and its mass is not predicted by the theory.

Experimental limits from direct searches at LEP indicate that the mass of the Standard Model Higgs boson must be larger than 114.4 GeV at 95% confidence level [9]. Indirect limits from electro-weak precision data put an upper mass limit at 185 GeV with 95% confidence level [10]. Combined results from many searches performed by the CDF and DØ collaborations at the Tevatron also exclude the presence of the Higgs boson at 95% confidence level in the mass range 158-175 GeV as of July 2010 [11]. Those limits are summarized in Figure 2.2. Both the Tevatron and LHC experimental collaborations are pursuing further studies to probe the remaining allowed mass range.

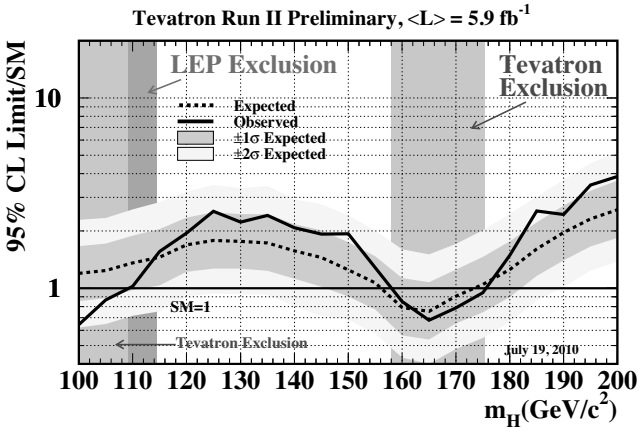

Figure 2.2: Experimental limits from direct searches of the Standard Model Higgs boson.

2.3.1 Extensions of the Higgs sector

While amazingly successful, the Standard Model cannot explain some of the observed phenomena in our Universe. For example, the amount of charge-parity violation needed to explain the dominance of matter in the Universe and the presence of dark matter cannot be accounted for in the Standard Model. As such, the Standard Model is often thought of as an effective theory, encased in a broader model that could account for the phenomenology currently left out. Of particular interest in the context of this thesis are models that contain an extension of the Higgs sector, resulting in the existence of not one, but many Higgs particles.

The simplest extension of the Higgs sector is to include a second Higgs complex scalar field doublet which has the same characteristics as the Standard Model one. This type of extension of the Higgs sector gives rise to a class of models called Two Higgs Doublet Models (2HDMs) [12]. There are now eight degrees of freedom in the Higgs sector, three of which are again used to give mass to the $W^{\pm}$ and Z^0 bosons. This leaves 5 remaining degrees of freedom which give rise to five physical Higgs particles: three neutral Higgs bosons and a pair of electrically charged Higgs bosons, $H^{\pm}$. This extension of the Standard model Higgs sector does not, by itself, provide enough new particle and interaction content to solve the issues of the Standard Model. However, this is the form that the Higgs sector takes in many of the models that do provide key components to describe new physics, such as for example, Supersymmetry [13]. Furthermore, the presence of a pair of charged Higgs bosons is experimentally appealing: their observation would be an unambiguous sign of physics beyond the Standard Model in a way that observation of a single neutral Higgs boson cannot be.

In the case that the mass of the charged Higgs is below $m_t - m_b$, the mass difference between the top and bottom quarks, the charged Higgs is called "light", and it can be produced in decays of the top quark, $t \to H^+ b$. Like the rest of the Higgs sector, a charged Higgs couples preferentially to heavier fermions. In most models, the preferred decay channel for a light charged Higgs is to a τ lepton via the process $H^+ \to \tau\nu$. The decay to quarks $H^+ \to c\bar{s}$ is also allowed but is the preferred decay channel only in certain limited areas in the model parameter space. The charged Higgs mass could also be heavier than that of the top quark. In that case, the production process occurs via gluon-gluon or gluon-bottom fusion. The decay channel to a τ lepton remains important but a new quark decay channel, $H^+ \to t\bar{b}$, opens up and quickly becomes the more dominant decay. Diagrams of the dominant production processes for charged Higgs bosons at the LHC are shown in Figure 2.3.

Before the start up of the LHC, direct searches were only possible for the case of a light charged Higgs, since a heavier charged Higgs was not experimentally accessible. At LEP, the ALEPH experiment excluded at 95% confidence level all masses below 79.3 GeV for all branching ratios in the top decays [15]. The Tevatron collaborations have attempted to measure directly

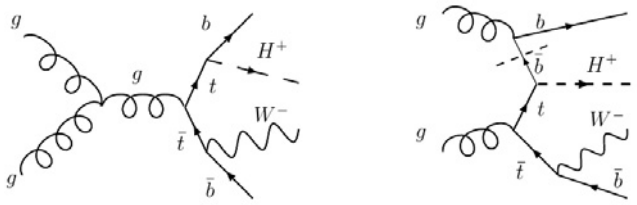

Figure 2.3: Dominant production processes at the LHC for charged Higgs bosons with a mass below (left) or above (right) that of the top quark. At the Tevatron, only the light charged Higgs is accessible, and the production mechanism is as shown on the left diagram, but with a $q\bar{q}$ pair instead of gluons as the initial particles [14].

the $t \to H^{\pm}b$ branching ratio. Current branching ratio upper limits vary between 10-30% depending on the mass of the charged Higgs and the chosen scenario for the decay of the charged Higgs [16, 17, 18]. Some recent limits from DØ are presented in Figure 2.4.

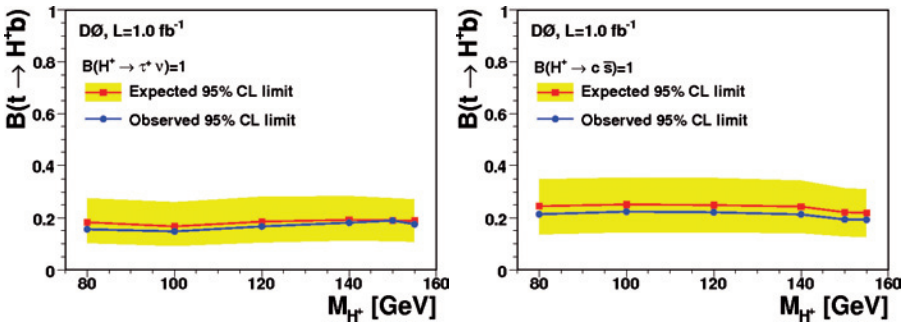

Figure 2.4: Experimental limits on the branching ratio of the top quark to a charged Higgs boson at DØ as a function of the charged Higgs mass. The charged Higgs is assumed to decay in all cases to $\tau\nu$ (left) or $c\bar{s}$ (right) and the top pair production cross-section is fixed [18].

The results listed above demonstrate clearly that the charged Higgs, if present in top quark decays, will be challenging to observe, in particular at the Tevatron where the sample of top quark events is limited by the small production cross-section. To extract such signal would require the use of sophisticated multivariate analysis methods. We have performed a preparatory study, presented in Paper III, of the potential of the Matrix Element method, one such powerful multivariate method, to be used for the measurement of the mass of a light charged Higgs boson. The method is also described in detail in Chapter 4.

3. Colliders and Detectors

Accelerator complexes and particle detectors are the tools used to make extensive and precise measurements in the field of high energy physics. This chapter provides an overview of the Fermilab accelerator complex and the DØ detector as well as the CERN accelerator complex and the ATLAS detector. Emphasis is put on the components that are used directly to obtain the results presented in the papers included in this thesis.

3.1 The Tevatron Collider at Fermilab

The Fermi National Accelerator Laboratory, also referred to as Fermilab, is located in Batavia, Illinois, and is home to the Tevatron collider. In the Tevatron, two beams, one of high energy protons and the other of high energy antiprotons, circulate in opposite directions along an accelerator ring with a circumference of 6.28 km. The Tevatron beams are produced by the accelerator complex shown in Figure 3.1. The production of the beams starts in a Cockroft-Walton accelerator [19, 20] where hydrogen gas is negatively ionized into H^- ions which are accelerated to an energy of 750 keV. The ions travel through successive stages of acceleration. Before injection into the Booster, they are stripped of their electrons, becoming a proton beam.

After they reach the Main Injector, protons can be extracted and made to collide with a nickel target for antiproton production. Antiprotons are separated from the rest of the collision products with a pulsed magnet. The antiproton beam is then bunched, focused and stored in the Accumulator ring or in the Recycler ring. When enough antiprotons have accumulated, proton and antiproton beams are injected in the Tevatron, where they are accelerated to 0.98 TeV per beam. Protons and antiprotons are made to collide at the center-of-mass energy of 1.96 TeV at two locations along the ring, where the DØ and CDF detectors are located. Each beam contains 36 bunches and collisions occur every 396 ns in each detector.

3.2 The DØ detector

The DØ detector [22] is a general purpose detector that records the result of high energy proton-antiproton collisions, also called events. The detector

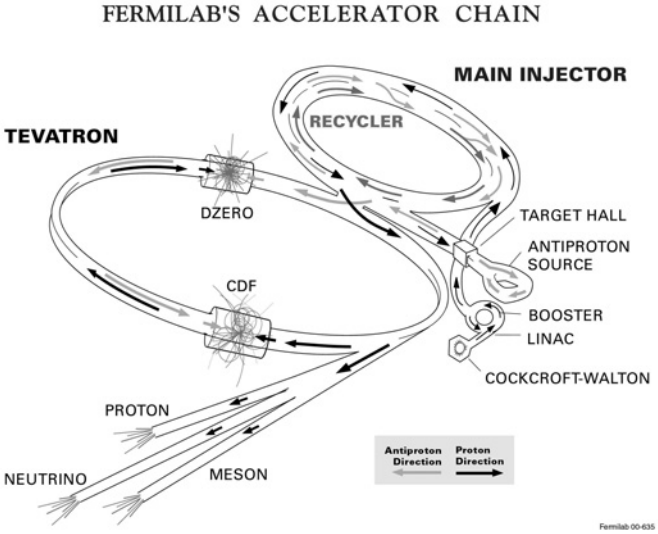

Figure 3.1: Schematic diagram of the accelerator complex at Fermilab [21].

measures the energy and direction of secondary particles produced in proton-antiproton collisions. The following sections describe the main components of the Run II DØ detector, from the center outwards. Figure 3.2 gives a schematic representation of the general detector layout.

The coordinate system used here defines the positive z direction parallel to the traveling direction of protons. The positive y direction points upwards and the positive x direction points toward the center of the Tevatron ring. Another coordinate definition is also used in which R is the radial coordinate in the plane perpendicular to the beam direction, ϕ is the azimuthal angle in this transverse plane and η is related to θ, the polar angle relative to the beam direction, by:

$$\eta = -\ln(\tan(\frac{\theta}{2})) \tag{3.1}$$

The pseudorapidity, η, is used instead of θ because it is a good approximation of the rapidity y when the velocity of the particle approaches the speed of light. The rapidity y is given by:

$$y = \frac{1}{2}\log\left[\frac{E + p_L}{E - p_L}\right] \tag{3.2}$$

where E is the energy of a particle and p_L its longitudinal momentum.

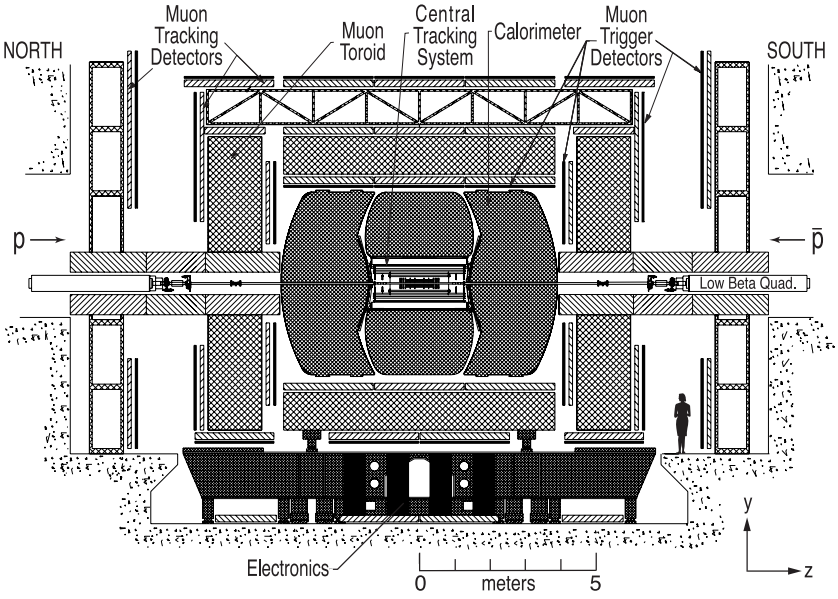

Figure 3.2: Schematic diagram depicting a cross-sectional view of the DØ detector.

3.2.1 The tracking system

The central tracking system is closest to the interaction region and measures the trajectory of charged particles resulting from high energy proton-antiproton collisions. A schematic diagram of the central tracking system is shown in Figure 3.3. Charged particles follow curved trajectories in the transverse plane of the tracking system because the tracking volume is enclosed in a superconducting solenoidal magnet producing a two Tesla magnetic field along the z direction. The curvature of the path followed by the traveling charged particle gives a measurement of the particle's transverse momentum. The central tracking system is composed of two distinct subsystems: the Silicon Microstrip Tracker (SMT) and the Central Fiber Tracker (CFT). The combined tracking resolution of the two subsystems for reconstructing the position of the primary interaction vertex is 35 μm along the x and y directions.

3.2.1.1 The Silicon Microstrip Tracker

The innermost tracking detector uses silicon microstrip technology to reconstruct particle tracks in the immediate vicinity of the interaction region. The Silicon Microstrip Tracker [23] at DØ is built from horizontal barrel sensors interspersed with vertical disk sensors, in order to maintain good coverage for tracking over the entire interaction region, irrespective of the exact position of the interaction point.

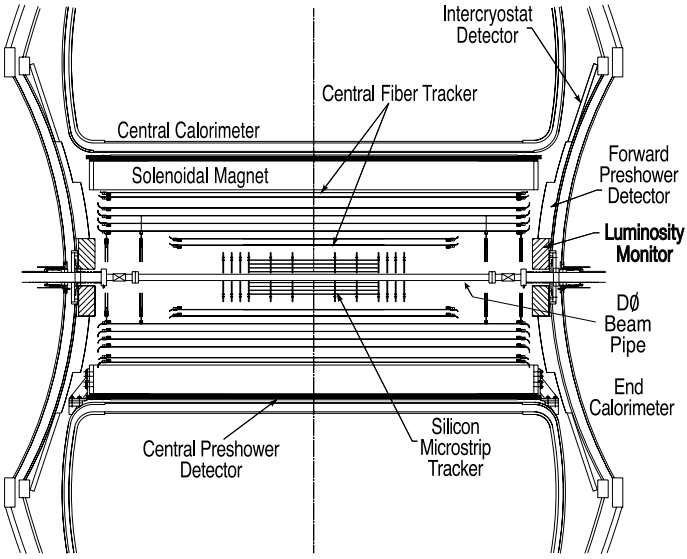

Figure 3.3: Schematic diagram of the cross-sectional view of the tracking volume of the DØ detector.

The six barrel sections are composed of four double-sided concentric layers. Hence, a charged particle traveling on a path perpendicular to the beam direction will leave eight barrel hits. The twelve central disks, called "F-disks", of inner radius 2.57 cm and outer radius 9.96 cm, are composed of "wedges" of double-sided silicon sensors and are located between $|z| = 12.5$ and 53.1 cm. Four so-called "H-disks" are located in the forward and backward regions at $|z| = 100.4$ and 121.0 cm. They have an inner radius of 9.5 cm and an outer radius of 26 cm and are composed of two layers of single-sided silicon sensors.

3.2.1.2 The Central Fiber Tracker

The Central Fiber Tracker [24] surrounds the Silicon Microstrip Tracker and occupies the radial space 20 cm $< R <$ 52 cm. It provides particle tracking in a large volume and contributes to the momentum measurement and the position reconstruction of charged particles in the event.

The Central Fiber Tracker is composed of eight cylindrical double layers of fluorescent dye scintillating fibers of radius 835 μm. In each double layer, one of the layers of fiber is mounted along the z-axis direction while the other is tilted at a stereo angle in ϕ of either +3^o or -3^o, alternating through the tracker, in order to provide three-dimensional position information. The Central Fiber Tracker covers the η range $|\eta| < 1.7$ with hits in all eight double layers.

The ends of the scintillating fibers are attached to clear waveguide fibers that bring the scintillator light signal to photon counters where the signal is read out. The $x-y$ position resolution on a double layer hit in the Central

Fiber Tracker is better than 100 μm. The transverse momentum resolution of the Central Fiber Tracker is approximately 7% for charged particles with transverse momentum of 50 GeV at $|\eta| = 0$.

3.2.1.3 Track reconstruction

A "reconstructed track", or often simply "track", is the name given to a series of hits in the tracking detector and their associated geometrical fit [25]. Signal-above-threshold in a tracking detector readout unit is called a "cluster". Once associated to a track, it becomes a "hit" for that track. Track reconstruction starts with a "hit candidate" in a given detector layer. Extrapolation to neighboring layers is attempted and if an appropriate cluster is found it becomes a hit candidate and the track kinematics are re-fitted with a Kalman filter update [26]. The process is iterated until a complete track is produced and added to the list of tracks for the event. If no kinematically viable track can be reconstructed, track finding restarts from a different hit candidate.

Up to 6 hits from the SMT and 8 hits from the CFT can be used to form a track. The tracking algorithm at DØ can reconstruct tracks down to a p_T of 180 MeV. However, at that low p_T, the reconstruction algorithms lose a lot of their efficiency. The tracking efficiency rises with p_T and reaches a plateau efficiency of approximately 95% around 500 MeV, as measured in simulated events during the study presented in Paper I.

3.2.2 The calorimeter system

The geometry of the DØ calorimeter system [27], a sampling calorimeter using liquid argon as its active material, can be seen in Figure 3.2. The central calorimeter (CC) is cylindrical and covers the region $|\eta| < 1$. The two end cap calorimeters (ECs) extend the region covered to about $|\eta| = 4$. Each of the CC and ECs contains three types of calorimeter cells. From the inside out, these are the electromagnetic (EM) layers, the fine hadronic (FH) layers and the coarse hadronic (CH) layers. The electromagnetic cells use depleted uranium as the target material whereas the fine hadronic layers use a uranium alloy with 2% niobium and the coarse hadronic layers use copper (CC) or stainless steel (ECs) plates. The thickness of the electromagnetic layers was designed such that all the particles in an electromagnetic shower are usually contained within the EM layers.

To improve the energy resolution and the coverage in the space between the CC and the ECs, additional sampling layers have been attached to the interior and exterior of the calorimeters' cryostats. This system is know as the Inter Cryostat Detector and Massless Gaps.

The main sources of noise in liquid argon calorimeters are electronic noise, uranium radioactivity and liquid Argon contamination by oxygen and nitrogen. At DØ, electronic noise in the coarse hadronic layers is the dominant source of noise in the calorimeter detector system.

3.2.3 The muon system

The muon detector system [28, 29] is the outermost subsystem of the DØ detector. The muon detector is divided in a central region and two end cap regions, forward and backward. The central muon system covers the range $|\eta| < 1$ and contains one toroid magnet of 1.8 T in the center and two toroid magnets of 1.9 T, one at each end of the detector. The central muon system consists of proportional drift tubes and scintillation counters. The drift tube system of the DØ muon detector has one layer of proportional drift chambers inside the toroid magnet (layer A) and two outside (layers B and C). The presence of the support structure of the detector prevents full solid angle coverage from being obtained. Approximately 55% of the central region is covered by the three proportional drift tube layers. The position resolution in the x and y directions for an individual layer hit in the proportional drift chambers is approximately 5 mm.

The forward and backward muon systems are composed of mini-drift tubes and scintillation counters. The mini-drift tubes extend the coverage of the muon system to $|\eta| \leq 2$. The position resolution of the mini-drift tubes is approximately 1 mm. The mini-drift tubes have a three-layer layout very similar to the proportional drift chambers in the central region. Figure 3.4 presents the layout of all the drift tubes in the central and end cap muon systems.

3.2.3.1 The muon trigger scintillators

In both the central and forward muon systems, the scintillation counters are used for trigger purposes because they provide a fast detector response. The scintillation counter layout is structured much like the drift tube layout with three layers in the forward and backward regions. In the central region there are two layers of scintillator. The so-called "A-ϕ" layer is attached to the innermost layer of proportional drift tubes and is used in the triggering. The cosmic cap is the external layer of the detector and it is used to veto cosmic ray events.

3.3 The Large Hadron Collider at CERN

The high energy physics laboratory of the European Organization for Nuclear Research, best known by its French acronym CERN, is located outside Geneva, at the French-Swiss border. It is home to the Large Hadron Collider (LHC) [30], the highest energy particle collider currently in operation. The original LHC design was for proton-proton collisions at center-of-mass energy of 14 TeV, but problems with the magnet system and an accident in September 2008 have, until now, prevented the LHC from producing 14 TeV collisions. The results and studies described in this thesis use data collected when two beams of protons where made to collide in the ATLAS detector at center-of-mass energies of 900 GeV and 7 TeV. The ATLAS detector is located at one

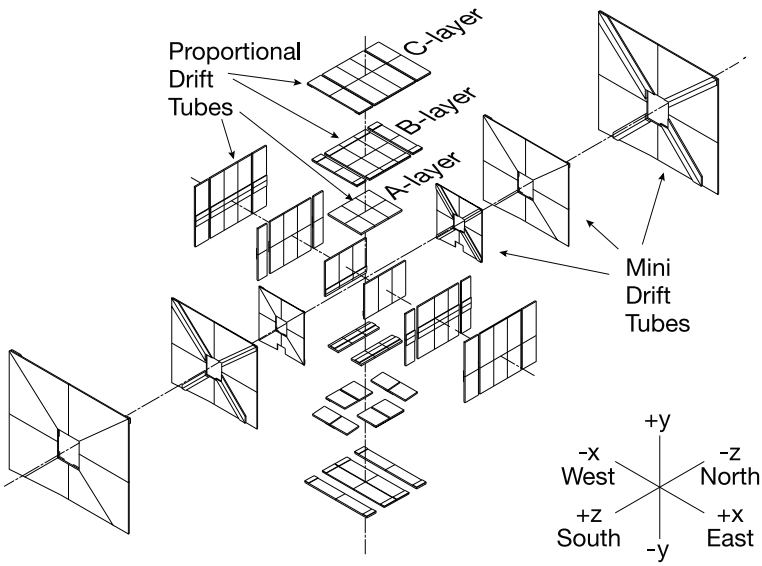

Figure 3.4: Schematic diagram of an exploded view of the drift chambers of the muon detector system of the DØ detector.

of the four collision points along the 27 km-long collider ring. The other collision points are home to the CMS, ALICE and LHCb detectors. The LHC is also designed for acceleration and collision of lead ions but this aspect is not discussed in this thesis.

The LHC is the last and highest energy stage of the CERN accelerator complex, shown in Figure 3.5. To produce the LHC beams, hydrogen gas is first stripped of its electrons, leaving protons that are injected into the LINAC-2, the first stage of acceleration. The beam then goes through the rest of the acceleration chain (BOOSTER, PS, SPS), where it is accelerated and also acquires its bunched structure, before being injected in the LHC, at an energy of 450 GeV per beam. Each beam can contain up to 2808 bunches and, with all bunches filled, a collision occurs every 25 ns. The final acceleration stage in the LHC takes approximately 20 minutes and the highest collision energy reached during data collection with proton beams in 2010 was 3.5 TeV per beam.

3.4 The ATLAS detector

ATLAS [32] is a general purpose detector located at one of the four collision points around the LHC. Similar in overall design to the DØ detector, it consists, radially outwards, of a tracking detector system, a calorimeter system and a muon detector system. Its coordinate system is defined like the DØ sys-

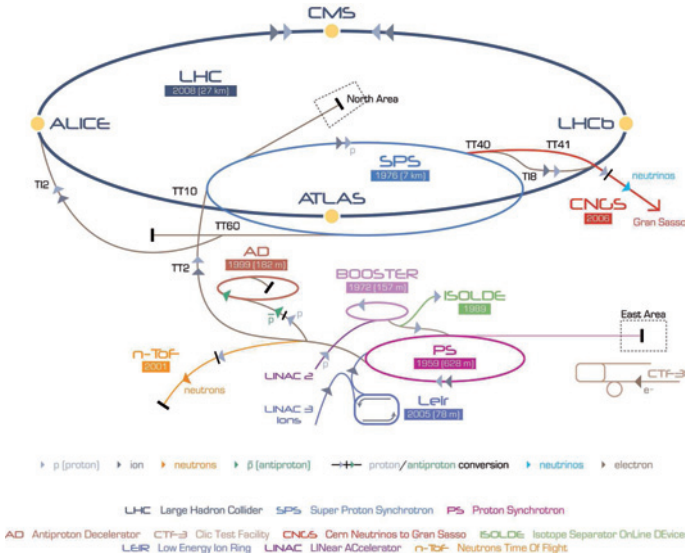

Figure 3.5: Schematic diagram depicting the CERN accelerator complex [31].

tem with the positive z-axis pointing along the beam line in the anticlockwise direction. An overview of the detector systems is shown in Figure 3.6.

3.4.1 The tracking system

The tracking system components are called collectively the Inner Detector [33], which is shown in Figure 3.7. From the center outward, the Inner Detector is composed of the Pixel detector, the Semi-Conductor Tracker (SCT) and the Transition Radiation Tracker (TRT). The Inner Detector is encased in a solenoid magnet that generates a 2 T magnetic field, curving the path of charged particles.

3.4.1.1 The Pixel Tracker

The Pixel detector is closest to the interaction point and offers coverage of the region $|\eta| < 2.5$ using high granularity silicon sensors. It is made up of three cylindrical barrel layers, parallel to the beampipe in the radial region $4.1 < R < 13$ cm, and 5 end cap disks per side that are perpendicular to the beampipe and have outer radii between 11 and 20 cm. The Pixel detector has an intrinsic resolution of 10 μm in $R-\phi$ and 115 μm in z.

3.4.1.2 The Semi-Conductor Tracker

The SCT is made up of a barrel with four double layers of silicon microstrips with a pitch of 80 μm, and 9 end cap disks per side. In the double layers of the barrel, one of the layers is at a 40 mrad stereo angle allowing determination

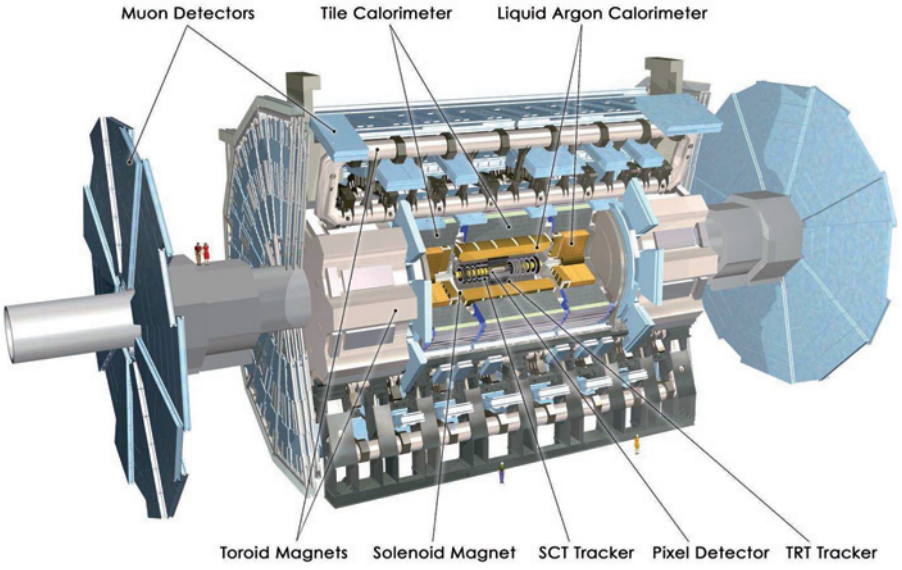

Figure 3.6: Schematic diagram depicting a cross-sectional view of the ATLAS detector.

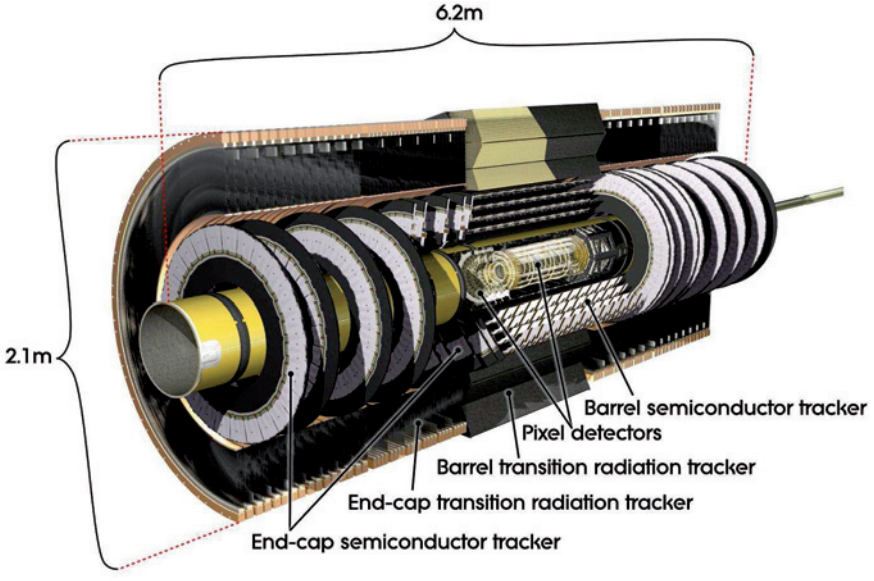

Figure 3.7: Schematic diagram depicting a cross-sectional view of Inner Detector at ATLAS.

of the position in z. The SCT barrel layers are located in the radial range 299 mm$<R<$514 mm. The SCT offers coverage of the region $|\eta|<$2.5 and has intrinsic resolution of 17 μm in $R-\phi$ and 580 μm in z.

3.4.1.3 The Transition Radiation Tracker

The TRT consists of a 144 cm long barrel and two end caps of 37 cm in radius, in which 4 mm straw tube detectors provide tracking points in $R-\phi$ only. The TRT covers the radial range 554 mm$<R<$1082 mm and can be used to reconstruct tracks in the region $|\eta| < 2.0$. The intrinsic resolution of an individual Xenon-filled straw is 130 μm. The large volume of the detector and densely packed straws can provide up to 36 tracking hits per track.

3.4.1.4 Track reconstruction

The procedure used for track reconstruction at ATLAS is very similar in concept to the one described for DØ in Section 3.2.1.3. However, the more extensive ATLAS tracking system can provide up to 3 or 5 hits in the Pixel detector, depending on location, up to 4 double hits or 9 single hits in the SCT, depending on whether the hits are in the barrel or in the disks, and up to 36 hits in the TRT. The track reconstruction can identify tracks with a p_T down to 100 MeV. However, the track reconstruction algorithms at low p_T are not very efficient, as measured via detailed studies on simulated events [34, 35]. The efficiency grows with p_T and reaches a plateau at approximately 85% around 1 GeV. The tracking efficiency is also best in the barrel region and decreases to reach approximately 60% close to $|\eta|$=2.5. The measured track reconstruction efficiency is important to the study presented in Paper II.

3.4.2 The calorimeter system

The ATLAS calorimeter system [36, 37] consists of electromagnetic (EM) calorimeters and hadronic calorimeters, and is also built on a barrel and end cap model. The EM barrel reaches radially out to 2.25 m and, with the EM end caps, provides coverage up to $|\eta| < 3.2$. The EM calorimeters use lead for the absorber layers and liquid Argon as the active material. The absorber layers have an accordion geometry. In the range $|\eta| < 2.5$, where tracking information is available, the granularity of the EM calorimeter is largest, to allow for precision matching of information between the calorimeter and the tracking detectors. The hadronic calorimeter system reaches radially out to 4.25 m and provides coverage up to $|\eta| < 4.9$. The barrel ($|\eta| < 1.5$) has iron absorber layers and active scintillating tile layers. In the hadronic end cap that extends the coverage to $|\eta| < 3.2$, the active material is liquid Argon and the absorber material is copper. The forward-most sections of the calorimeter also use liquid Argon, and the absorber layers are either copper or tungsten.

3.4.3 The muon system

The ATLAS muon spectrometer [38] is encased in a system of air-core toroid magnets. The central eight coils provide a peak field of 3.9 T while the end cap toroids provide a peak field of 4.1 T. The bulk of the spectrometer is composed of drift tube detectors in three layers to provide a track curvature measurement in the range $|\eta| < 2.7$. In the higher pseudorapidity region $|\eta| > 2$, the first detector layer is composed of higher granularity cathode strip chambers, multiwire proportional chambers that perform better under the higher particle flow in the forward direction. Resistive plate chambers (in the barrel) and thin gap chambers (in the end cap), that have faster readout capability than the drift tubes, are used for trigger purposes. Some of their layers are perpendicular to the drift tube planes, providing complementary spatial information along the drift wire axis.

3.4.4 The trigger system

At nominal running conditions, the LHC provides 40 MHz of collisions to the ATLAS detector. However, only up to 200 Hz are available to record data for analysis so it is the task of the trigger system to reduce, in real time, the data stream to match the recording bandwidth. In order to achieve the necessary rejection power, a system of three successive filtering layers is used. The first level trigger (L1) [39], is entirely hardware-based to achieve low latency. The L1 decision is determined from the data provided by the parts of the detector that have the fastest readout electronics, which include the muon system and a specialized low-granularity calorimeter readout. The L1 latency is 2.5 μs and the event rate out of L1 is reduced to approximately 100 kHz. The L1 trigger result contains a list of Regions of Interest (RoIs) that indicate areas where activity was detected at L1.

The second and third levels of the trigger are collectively called the High Level Trigger [40]. The second level of the trigger (L2) is software-based and has access to the full detector readout data in the RoIs provided by L1. The latency available to take the decision is approximately 40 ms so simple object reconstruction using full granularity data is possible. The output rate out of L2 is approximately 3.5 kHz. Finally, the last trigger level is the Event Filter (EF). It is also software-based. There, the detector data for the entire event is available and a full event reconstruction is done, using reconstruction algorithms that mimic as closely as possible the offline reconstruction. The EF latency is 1-4 s and the output rate is 100-200 Hz. Events that satisfy the EF requirements are permanently stored and distributed around the world for analysis.

3.4.4.1 The minimum bias trigger

The minimum bias trigger [41] is a special case in the trigger system, and is meant to select an event sample that is as unbiased as possible relative to

the overall event mixture produced by LHC proton-proton collisions. It is the trigger used to collect the sample analyzed in Paper II. At L1, the minimum bias trigger takes its input from two specific hardware devices: Beam Pickup Timing devices (BPTX) and Minimum Bias Trigger Scintillators (MBTS). The BPTX are electrostatic beam pickup devices located ± 175 m along the beampipe from the center of the ATLAS detector that are used to assess the presence of proton bunches during a particular collision timing window. The MBTS is a 2 cm-thick polystyrene scintillator detector located at ± 3.56 m from the center of the ATLAS detector, in front on the end cap calorimeters. On each side, the MBTS is a disk, 89 cm in radius, perpendicular to the beam direction with two rings with η coverage $2.09<|\eta|<2.82$ and $2.82<|\eta|<3.84$. Each ring is further divided into 8 azimuthal sectors for a total of 32 scintillators in the MBTS detector. A schematic representation of the MBTS layout is shown in Figure 3.8. The requirement for the minimum bias trigger to fire is the coincidence of signal-above-threshold in the BPTX and at least one scintillator. It is possible to require L2 confirmation of the scintillator hit via the more refined L2 readout and electronics or to combine this L1 requirement with requirements on tracker hits or track presence at L2 and in the EF.

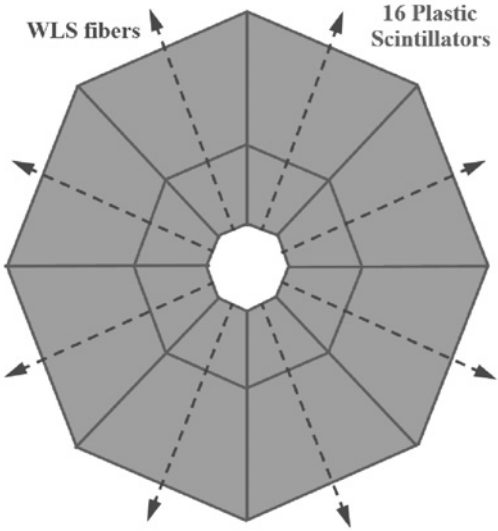

Figure 3.8: Schematic representation of the ATLAS MBTS.

3.4.4.2 The τ trigger

The ATLAS trigger and data acquisition systems also attempt to select and record events that contain moderate- to high-p_T τ leptons [42]. This is done by looking for hadronic decays of the τ into one (1-prong) or three (3-prong) charged pions or Kaons in the data. The cases where the τ lepton decays to one or more lighter leptons (electrons or muons) do not fall in the category called

"τ trigger" but in the other "leptonic trigger" categories. The main challenge of the τ trigger is to reject QCD jets while remaining as efficient as possible in selecting events with true τ leptons.

The typical signatures of an hadronically-decaying τ lepton consist of one or three charged particle tracks in the Inner Detector and an energy cluster in the calorimeter system. At L1, only calorimeter information is available to make a τ trigger decision [43]. This information is available in the form of approximately 7200 trigger towers measuring 0.1×0.1 in $\eta - \phi$ space, with one readout from the EM layers and one from the hadronic layers. A 4-tower sliding-window algorithm then runs over the calorimeter towers, constituting a potential RoI. At each step, four hadronic clusters are created by summing the EM and hadronic energies of pairs of adjacent towers, as is shown in Figure 3.9. Then, the energy of each cluster is checked against the trigger thresholds. If an isolation requirement is present, the 12 towers surrounding the sliding-window core are also used. Their total energy (EM+hadronic) is summed over and compared to the isolation requirement if present. Finally, as the sliding-window algorithm progresses over the calorimeter, the energy of a given potential RoI is compared to that of its neighboring and overlapping RoI candidates, and is selected as a RoI only if it is a local maximum.

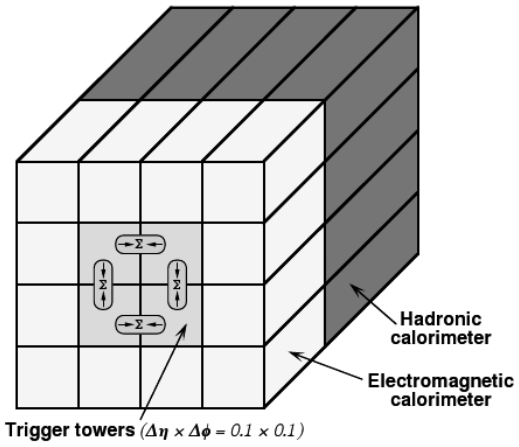

Figure 3.9: Trigger towers and sums used in the L1 τ trigger sliding-window algorithm.

At L2, the trigger system accesses the detector information for the RoIs provided by L1. A more refined reconstruction of the characteristics of the τ candidates is done and many more properties can be considered to reach a trigger decision. In particular, narrowness of the calorimeter cluster, multiplicity (one or three) of associated tracks and a more refined isolation calculation can be called upon. The improved energy measurement can also affect the decision. The background rejection factor of L2 is improved by a factor of approximately 20 relative to L1.

Finally, the EF proceeds to recalculate the characteristics of τ candidates using exactly the procedure used in the offline software. However, in view of the limited time available to the trigger, the algorithms are seeded with the L1/L2 RoIs. Two algorithms are used, one that does a calorimeter-driven reconstruction and identification, and one that is track-driven. The results of the two algorithms are then merged in one list of τ candidates that are evaluated in relation to the trigger criteria. With this detailed reconstruction, more characteristics of the τ candidates can be used in the trigger decision. The "electromagnetic radius" characterizes the narrowness of the shower and is an especially good discriminator for lower transverse energy (E_T) τ candidates. The isolation criteria can also be made very tight to take advantage of the narrowness of the calorimeter clusters from real τ leptons. The number and energy of the hits in the first and highest granularity layer of the calorimeter can be used. The number of associated tracks and the sum of the charge of the tracks are a tool to ensure the presence of good 1- or 3-prong decay candidates. The "lifetime signed impact parameter" combines information from the track impact parameter and jet axis to check that the decay occurs in the flight direction and is particularly efficient in rejecting QCD background for τ candidates with high E_T. Finally, the ratio of the p_T of the τ candidate to the p_T of the leading track is expected to be large in real τ leptons and is another criterion that is available in the trigger decision.

Measurements of the trigger efficiency are necessary to be able to use events selected with a τ trigger in any analysis. A data-driven method to measure the τ trigger efficiency using events in which a Z boson is produced and decays to $\tau^+\tau^-$ was studied in the context of the first LHC data. This study is presented in Paper IV.

4. The Matrix Element method

4.1 Overview

The Matrix Element method is a multivariate analysis technique that aims at extracting the most precise measurement of a given quantity from a statistically limited event sample by using all the kinematic information contained in this sample. The first analysis performed with this method was a measurement of the top mass at the Tevatron, see [44]. The method will be described briefly in this chapter. More detailed descriptions can be found in [45, 46, 47]. The properties of the method make it a good candidate for determining the mass of the charged Higgs if and when there is some first evidence of its existence and the number of signal events is still very limited. In Paper III, we present a study of the potential of the Matrix Element method to provide a charged Higgs mass measurement in the electron decay channel shown in Figure 4.1.

This is a preliminary feasibility study that was performed using simulated DØ signal-only events and the MadWeight software package [48]. It focuses in particular on the use of a transfer function to describe the τ decay chain.

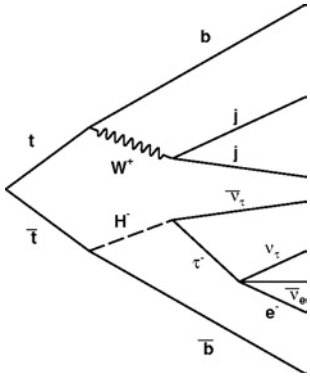

Figure 4.1: Diagram of the process of light charged Higgs production in $t\bar{t}$ decays with τ decay to a final-state electron.

4.2 The likelihood

The principle on which the Matrix Element method is built is that the probability of a given physical process producing a given event or set of events can

be calculated if the Matrix Element for this process is known. We start with a set of model parameters α (in our case, the mass of the charged Higgs boson), to be measured. We define x to be a full set of event measurements and y to be that same set of quantities but at partonic level. The matrix element-weighted probability is then

$$P(x,\alpha) = \frac{1}{\sigma_\alpha} \int d\phi(y) dz_1 dz_2 f(z_1) f(z_2) |\mathscr{M}_\alpha|^2(y) T(x,y) \tag{4.1}$$

where $1/\sigma_\alpha$ is a cross-section normalization factor that ensures that $P(x,\alpha)$ is a well-defined probability density, $d\phi(y)$ is the multi-dimensional phase-space integration measure, $f(z_1)f(z_2)$ are the parton distribution functions for the two incoming partons, which are also integrated over, $|\mathscr{M}_\alpha|^2(y)$ is the squared matrix element amplitude and $T(x,y)$ is the resolution or transfer function that relates the experimentally measured quantities to the partonic quantities. Transfer functions are discussed in detail in Section 4.4.

A likelihood maximization procedure is performed to obtain the best estimate of the model parameters α. For N events, the differential likelihood to be maximized is given by

$$\mathscr{L}(\alpha) = e^{-N\int \bar{P}(x,\alpha)dx} \prod_{i=1}^{N} \bar{P}(x_i,\alpha) \tag{4.2}$$

where $\bar{P}(x,\alpha)$ is the measured probability density. It is related to the generated probability density by the relationship

$$\bar{P}(x,\alpha) = Acc(x) P(x,\alpha) \tag{4.3}$$

where $Acc(x)$ is a term that describes the detector acceptance and depends only on the kinematic properties of the events.

The likelihood $\mathscr{L}(\alpha)$ is typically a rapidly-varying quantity which makes direct maximization unpractical. Instead, $-\ln\mathscr{L}$, given by

$$-\ln\mathscr{L}(\alpha) = -\sum_{i=1}^{N} \ln\bar{P}(x_i,\alpha) + N\int \bar{P}(x,\alpha)dx \tag{4.4}$$

$$= -\sum_{i=1}^{N} \ln[P(x_i,\alpha)Acc(x_i)] + N\int Acc(x)P(x,\alpha)dx \tag{4.5}$$

is minimized. The term $-\sum_{i=1}^{N}\ln Acc(x_i)$ does not depend on α and thus can be omitted from the likelihood maximization calculation. The integral $\int Acc(x)P(x,\alpha)dx$ can be estimated from fully simulated Monte Carlo events to be the ratio of the number of events that are accepted after the full selection, N_{acc}, to the number of events that were generated by the simulation program,

N_{gen}, as a function of α, which can be expressed as

$$\int Acc(x)P(x,\alpha)dx = \frac{N_{acc}}{N_{gen}}(\alpha). \tag{4.6}$$

The function to be minimized then becomes

$$-\ln\mathscr{L}(\alpha) = -\sum_{i=1}^{N}\ln P(x_i,\alpha) + N\cdot\frac{N_{acc}}{N_{gen}}(\alpha) \tag{4.7}$$

where all terms independent of α have been omitted.

To do a measurement of α for a given signal process in the presence of background, the probability must be computed that events not only belong to the signal process (P_{sgn}) but also to every background process that contributes significantly to the event sample under consideration (P_{bkg}). The probabilities must be included in the likelihood by letting, for example in the case of only one background process,

$$P(x_i,\alpha) = f\cdot P_{sgn}(x_i,\alpha) + (1-f)P_{bkg}(x_i,\alpha) \tag{4.8}$$

where f is the fraction of signal events in the sample. The parameter f is fitted at the same time as α in the overall likelihood maximization.

4.3 MadWeight

MadWeight [48] is a software package in the MadGraph/MadEvent suite. Its goal is to facilitate analysis with the Matrix Element method by providing an efficient phase-space generator for the computation of the matrix element-weighted probability using Monte Carlo integration methods. MadWeight is integrated with the software suite. The matrix element of the process investigated is generated with MadGraph. The analyst must then provide the transfer functions that describe their experimental setup and the data in the "LHC Olympics" format [49] which is required by MadWeight. The study was performed using MadWeight version 2.1.11 and the associated version of MadGraph. In this version, the full $2 \to 8$ matrix element of the process in Figure 4.1 has too many internal propagators to be generated with MadGraph. Thus, we chose to use the $2 \to 6$ matrix element in which the τ is kept undecayed and to treat this decay with a transfer function. This process is described in detail in Section 4.4.2.

4.4 Transfer Functions

The value of the transfer function $T(x,y)$ varies rapidly over small regions in the phase space, giving it a structure in spikes that makes the integration of the probability in Equation 4.1 challenging. The function can be factorized as a product of individual transfer functions for every kinematic parameter of each measured final state particle. Thus, for a final state with n measured particles, the transfer function can be expressed as

$$T(x,y) = \prod_{i=1}^{n} T_i(x_i,y_i) = \prod_{i=1}^{n} \left[T_i^E(x_i,y_i) T_i^\eta(x_i,y_i) T_i^\phi(x_i,y_i) \right] \tag{4.9}$$

where x_i and y_i are, respectively, the experimentally measured and partonic kinematic properties of each final state particle and T_i is the transfer function associated to each particle, which can vary according to particle type. Each T_i can be factorized further into an energy component T_i^E and two spatial components, T_i^η and T_i^ϕ, for a complete description of the particle kinematics. Neutrinos are a special case for the transfer function, since they are not measured. They have $T_i = 1$. In our study, since the DØ detector can provide very accurate position measurements, the spatial components T_i^η and T_i^ϕ are chosen to be δ-functions for all final state particles. The energy component T_i^E was studied in more detail and is described in the next two subsections.

4.4.1 Jet transfer functions

The relationship between the measured energy of a particle jet and the original parton that produced it, quark or gluon, is complex. The dominant factor that affects this relationship is the fact that the DØ calorimeter is a sampling calorimeter. Only some of the volume in which energy is deposited is instrumented and the energy measurement must be corrected to account for this effect employing the so-called Jet Energy Scale (JES) correction [50]. Other factors such as energy losses to invisible particles, calorimeter noise and thresholds also affect this relationship. After the JES correction has been applied, the mean energy difference between the partonic and experimentally measured jet energies is zero, but the distribution of the energy difference δ_E between E_{JES}, the energy of a JES-corrected jet, and E_{parton}, the energy of the parton that created the jet, has a large, asymmetrical width. Observation of simulated DØ events shows that the δ_E distribution is different in the three structural regions of the calorimeter system and can be parametrized with a distribution which is the sum of two Gaussians. Furthermore, this distribution is energy-dependent. The variation of the parameters of the double-Gaussian is approximately linear with energy. We also observe that the distributions are different for light jets (u, d) and for b-jets. This energy-dependent double Gaussian is chosen to be the transfer function. To be a proper transfer function, it must be normalized. The jet transfer function can thus be expressed

as

$$T(\delta_E) = \frac{1}{\sqrt{2\pi}(p_2 + p_3 p_5)} \left(e^{\frac{-(\delta_E - p_1)^2}{2p_2^2}} + p_3 \, e^{\frac{-(\delta_E - p_4)^2}{2p_5^2}} \right) \tag{4.10}$$

where $p_{1..5}$ are fitted parameters. To determine $p_{1..5}$, we fitted Monte Carlo simulated δ_E distributions binned in E_{JES} for the central, intercryostat and endcap regions of the calorimeter with Equation 4.10, replacing the normalization coefficient with an amplitude parameter. The procedure was performed twice, once for a sample of charged Higgs events and a second time with a sample of Standard Model $t\bar{t}$ events. A linear fit was done for each parameter as a function of the average E_{JES} in each of the δ_E distributions. This process was done separately for light jets and for b-jets in each of the three detector regions. The signal sample and the $t\bar{t}$ sample yielded compatible transfer function parameters, as expected, since the transfer function reflects properties of the detector and should be independent of the physics process simulated in the sample used to derive it.

4.4.2 Electron/τ transfer functions

As mentioned previously, the limitations of MadGraph prevent the inclusion of the τ decay in the matrix element used in the probability calculation. Instead, the matrix element of the $2 \rightarrow 6$ process to a stable τ is used. However, the information available in the detector is that of the measured electron resulting from the τ decay. To be able to calculate the probabilities for events of the type shown in Figure 4.1, we have calculated a transfer function that not only accounts for the detector effects in the reconstruction of the electron but also the effects associated to the τ decay. The τ resulting from the decay of a charged Higgs is highly boosted which results in the electron being well aligned in space with its parent τ, as can be seen in Figure 4.2. It is a good approximation to keep the spatial components of the transfer function T_τ^η and T_τ^ϕ as δ-functions. There is, however, a very large energy difference between the measured electron and the τ. A study of the Monte Carlo simulated distribution of the energy difference between the τ and the observed electron have lead to the conclusion that the shape of the distribution is similar to that of the Landau distribution for which the analytical Moyal formula is a good approximation that can be implemented as the transfer function in MadWeight.

The Moyal function, normalized to unit area, is given by

$$T_\tau(D) = \sqrt{\left(\frac{e^{-(p_2(D-p_1) + e^{-p_2(D-p_1)})}}{2\pi} \right)} \tag{4.11}$$

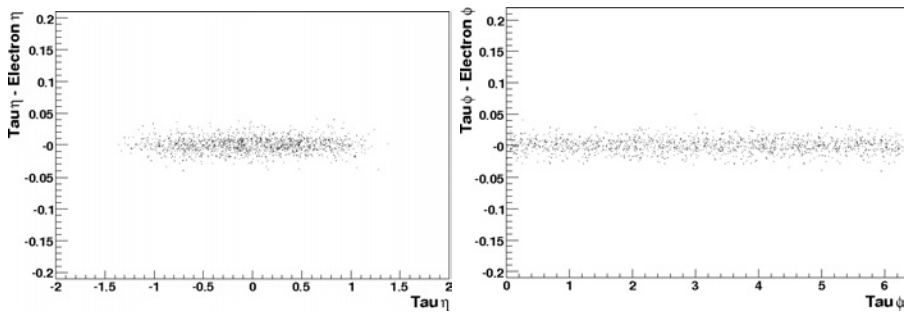

Figure 4.2: Position difference in η (left) and ϕ (right) between generated τ leptons and their reconstructed daughter electrons as a function of the τ position in the respective coordinate.

where $D = E_\tau - E_e$ is the energy difference between the τ and the measured electron and p_1 and p_2 are fitted parameters. The parameter p_1 is the most probable value for D and p_2 is related to the width of the distribution. Two fits were performed using simulated events with e^+ and e^- respectively. The two fits gave compatible results.

The results of the application of the transfer functions presented here on the reconstruction of the charged Higgs mass in simulated events at DØ are presented in detail in Paper III.

5. Summary of papers

5.1 Paper I

Study of ϕ and η correlations in minimum bias events with the DØ detector at the Fermilab Tevatron Collider

In this paper we study angular correlations between charged particle tracks reconstructed with the tracking detector of the DØ experiment in a minimum bias event sample. This sample is constructed by taking advantage of the fact that more than one collision can occur in a single bunch crossing. If one collision triggers the event to be recorded, other interactions in this crossing can be considered minimally biased. Two new observables have been designed and used for this study. In the so-called "crest shape" observable, correlations in the azimuthal angle, ϕ, between the track with the largest transverse momentum in the event and each one of the other tracks, are studied. A dual peak structure is observed in the $\Delta\phi$ distribution, with enhancements at zero and π. They can be interpreted as an emerging di-jet structure at the softest level. We compare this "crest shape" to various PYTHIA tunes. We find that tunes which include more contributions from hard, perturbative calculations than soft, non-perturbative modeling better match this shape.

The second observable, called "same minus opposite", also incorporates correlations in pseudorapidity (η) by considering separately the azimuthal angle correlation distributions for tracks that lie in the same η half of the detector as the leading track and those that lie in the opposite half. Subtracting the "opposite" distribution from the "same" distribution, we observe a shape with a large peak close to zero. The distribution in the rest of the $\Delta\phi$ range stays above zero, indicating that more tracks are present in the "same" region across the whole $\Delta\phi$ range. No tune studied in this paper can fully describe this effect, but tunes that use transverse momentum-ordered showering algorithms describe this effect qualitatively much better than tunes using virtuality-ordered showering.

Both observables were designed to be especially robust against experimental and detector effects. This makes the resulting distributions useful for comparison with current tunes and a possible input for further tuning of soft QCD and multi-parton interaction models.

5.2 Paper II

Angular correlations between charged particles from proton-proton collisions at $\sqrt{s}$=900 GeV and $\sqrt{s}$=7 TeV measured with the ATLAS detector

The same two observables as in Paper I are studied using data collected with the ATLAS detector at the two collision energies $\sqrt{s}$=900 GeV and $\sqrt{s}$=7 TeV. The data samples were collected using a minimum bias trigger. Extensive comparisons to PYTHIA tunes are made and we observe again that the models and tunes do not describe well the data. The distributions, in particular those obtained with the larger 7 TeV sample, have small statistical and systematic errors. They can be used for further tuning of Monte Carlo event generators.

5.3 Paper III

Transfer function treatment of leptonic tau decays in the Matrix Element method

We use simulated events to investigate the potential of the Matrix Element method, in particular as implemented in the MadWeight software package, as a method to measure the mass of the charged Higgs boson, if present in top quark decays. The decay channel used in this study is $H^{\pm} \to \tau^{\pm}\nu \to e^{\pm} + 3\nu$. The study focuses on the inclusion of the τ decay via a transfer function. This is a preparatory study that indicates that an accurate measurement via this method should be possible. However, further studies are necessary to assess the accuracy and resolution using more realistic experimental conditions, in particular by including background events in the simulated event sample.

5.4 Paper IV

The ATLAS tau trigger and planned trigger efficiency studies with early data

This paper presents an overview of the ATLAS trigger for hadronically decaying τ leptons and the trigger menus planned for early data. The focus of the paper is a Monte Carlo study of a tag-and-probe method to measure the τ trigger efficiency once 100 pb^{-1} of data has been collected. In this method, we select a high purity sample of Z bosons that decay to a τ pair were one of the τ leptons decays hadronically and the other one decays to a μ and two neutrinos. The μ side is the tag side and the hadronic side is the probe side. This tagging allows us to select a sample without biasing it relative to the hadronic τ trigger or any of the detector components that are used in the hadronic τ trigger. We calculate the trigger efficiency as the ratio of the number of τ leptons found

by the trigger on the probe side over the number of τ leptons identified in the offline reconstruction. We conclude from this study on simulated data that the method can provide a measurement of the trigger efficiency of satisfactory accuracy with as little as 100 pb^{-1} of data.

6. Summary in Swedish

Vinkelkorrelationer i ”minimum bias”-kollisioner och förberedande studier för sökandet efter den laddade Higgsbosonen vid Tevatron- och LHC-kolliderarna

Inom elementarpartikelfysiken utforskas materiens minska beståndsdelar och deras växelverkningar. Den generella teori som används för att tolka experimentdat”a är baserad på relativistisk kvantfältteori och kallas för Standardmodellen. Standardmodellen beskriver tre av de fyra krafterna i universum: den elektromagnetiska växelverkan, den svaga växelverkan och den starka växelverkan. Gravitationen beskrivs av den generella relativitetsteorin och är inte inkluderad i Standardmodellen.

Standardmodellen och den laddade Higgsbosonen

Standardmodellen beskriver två typer av partiklar: fermioner och bosoner. Fermionerna bygger upp universums materia och kan antingen vara leptoner (elektroner, myoner, tauoner och deras neutriner) eller kvarkar (upp-, ner-, sär-, charm-, topp- eller bottenkvarkar). Bosoner är partiklar som förmedlar kraftväxelverkan medan fermionerna. Fotoner förmedlar den elektromagnetiska växelverkan mellan elektriskt laddade partiklar, W- och Z-bosoner förmedlar den svaga växelverkan som orsakar radioaktiva sönderfall och gluoner förmedlar den starka växelverkan. Den starka växelverkan håller ihop kvarkarna så att de bildar protoner och andra s.k. hadronpartiklar.

Den del av Standardmodellen som beskriver den starka växelverkan kallas kvantkromodynamik (på engelska ”Quantum Chromodynamics”, QCD). För att undersöka den starka växelverkan kan man bl.a. studera så kallade ”minimum bias”-kollisioner. I denna avhandling har vinkelkorrelationer mellan laddade partiklar i ”minimum bias”-kollisioner studerats med hjälp av två olika partikeldetektorer: DØ- och ATLAS-detektorerna. Resultaten av dessa studier återfinns i Artikel I och II. För att uppnå bästa möjliga resultat i analysen av experimentdata måste vi också ha simulerade data att jämföra med. I de s.k. ”mjuka” kollisioner, som vi har studerat, sker simuleringen med användning av speciella modeller för den starka växelverkan istället för med den generella QCD-teorin. Detta beror på att QCD bryter samman och slutar fungera för beskrivningen av mjuka kollisioner. Resultaten visar att de speciella modeller som används f.n. inte ger en god beskriving av de vinkelkorrelationer som vi observerar i experimentdata.

Det finns ytterligare en boson i Standardmodellen vilken hittills inte observerats: Higgsbosonen. Denna partikel är oladdad och ger enligt Standardmodellen upphov till massan hos alla andra partiklar genom den s.k. Higgsmekanismen. Vidare kan Standardmodellen som generell teori inte vara komplett eftersom den, bl.a., inte kan förklara förekomsten av universums mörka materia. För att vidareutveckla Standardmodellen kan man t.ex. utöka Higgssektorn. Med två Higgsfält, istället för ett enda som i Standardmodellen, får man fem Higgsbosoner istället för en. Tre av dessa bosoner är oladdade och två är laddade. Observation av en laddad Higgspartikel skulle påvisa förekomsten av fysikaliska fenomen bortom de som beskrivs av Standardmodellen i dess nuvarande form. Om den laddade Higgspartikeln visar sig vara lättare än toppkvarken, som har en massa på 172 GeV, kan den skapas i toppkvarkens sönderfall via processen $t \rightarrow H^{+}b$. Resultaten från LEP-experiment visar att den laddade Higgspartikeln, om den existerar, måste ha en massa som är större än 79,3 GeV. Det är viktigt att studera och utveckla nya kraftfulla dataanalysmetoder med vilka det är möjligt att upptäcka den laddade Higgsbosonen och bestämma dess massa. I Artikel III använder vi simulerade data för att studera laddade Higgspartiklar i toppsönderfall med hjälp av den s.k. matriselementmetoden för att se om denna metod kan användas för att mäta den laddade Higgspartikelns massa med god precision. Det är en förberedande studie med vissa förenklingar. Vår slutsats är att det sannolikt går att använda metoden för detta syfte, men att ytterligare studier krävs för att säkerställa detta.

Acceleratorer och detektorer

På Fermi National Accelerator Laboratory utanför Chicago finns den s.k. Tevatronacceleratorn. I denna låter man en protonstråle kollidera med en antiprotonstråle vid en energi av 1,96 TeV. Två stora detektorer, CDF och DØ (uttalas ”D-noll”), detekterar de partiklar som produceras vid kollisionerna. I Artikel I analyseras experimentdata från DØ-data. I Artikel III analyseras simulerade DØ data.

På CERN-laboratoriet utanför Genève finns LHC-acceleratorn, med två protonstrålar som leds runt åt motsatt håll. I fyra punkter låter man strålarna kollidera med varandra och vid varje sådan punkt finns en detektor: ALICE, ATLAS, CMS och LHCb. Kollisionsenergin kan varieras. För resultaten i Artikel II har data från ATLAS insamlade vid energierna 900 GeV och 7 TeV studerats.

DØ- och ATLAS-detektorerna är uppbyggda på likartat sätt. I centrum av detektorn finns en spårdetektor som mäter riktning och röreslemängd för de laddade partiklarna. Denna detektor omges av en kalorimeter i vilken neutrala och laddade partiklar avsätter hela sin energi. Det yttre lagret av detektorn mäter röreslemängden hos myoner.

LHC-acceleratorn kan ge upphov till 40 miljoner proton-protonkollisioner i ATLAS-detektorn per sekund. De flesta av dessa kollisioner utgörs av välkända kollisionprocesser. Eftersom lagringen av alla kollisionsdata skulle uppta alldeles för mycket datalagringsutrymme, så finns ett s.k. triggersystem som

väljer ut bara vissa kollisioner som sparas för analys. Triggersystemets uppgift är att identifiera och spara kollisioner med interessanta fysikprocesser. Systemet gör dessa bl.a. genom att välja ut kollisioner med partiklar som har mycket hög energi. En av de partiklar som vi vill identifiera i triggersystemet är τ-leptonen vilken uppstår bl.a. då den laddade Higgsbosonen sönderfaller. I Artikel IV studerade vi en metod för att mäta triggereffektiviteten för kollisioner som innehåller en τ-lepton. Slutsatsen är att metoden fungerar bra och att den kommer att kunna användas i ATLAS.

7. Acknowledgments

First, my thanks go out to my thesis advisors Tord and Claus who lead by example and provided a great mixture of support and enthusiasm. Claus, your scientific creativity means that every discussion with you is thought-provoking. Tord, you are the pillar upon which this group is built and our successes would not be possible without you.

I would like to thank the other members, past and present, of the experimental particle physics group: Richard, Enzo, Charlie, Daniel, Bjarte, Mattias, Markus and Nils. Your support has been very valuable. I have to make a special mention for Elias and Martin, my office mates, travel partners and partners in mischief. My time in Uppsala and at CERN would not have been the same without you, both from a scientific and a personal point of view.

It has been fantastic to be able to work in close collaboration with the phenomenology group, and I would like to thank Gunnar, Johan, Rikard, Nazila and Roman for always keeping their doors open. Special thanks go to the group's doctoral students Oscar and David with whom scientific discussions have always been enriching and who have also become dear friends.

Sophie, what a pleasure it has been to be your gym partner: I will miss those bruises! Your dedication to fitness is inspiring, and I have enjoyed every minute of our friendship. Thank you also for your infinite patience for my mangled Swedish!

P-A, thank you for all the fikas and for letting me join you on the roof whenever I needed a little pause.

Karl-Johan, thank you for being the only other member of our 2-people thesis support group. It was nice to chat with someone who understood exactly what I was going through.

I would like to thank all of the other researchers at the department that contribute to the lively atmosphere, in particular Tord J., Volker, Roger and Tomoko.

Many thanks to all the other research students, in particular the other doctoral students, for discussions and friendships that I will never forget: Patrick, Erik, David D., Henrik J., Henrik P., Magnus, Andrea, Karin, Agnes, Peder, Glenn, Dominik, Olle, Martino, Karla, Karl-Oscar, Stephan, Aila, Lena, Kristoffer, Mikaël, Bengt, Alexander... and as I am quite certain that some names are missing, know that it is not because I do not count you as a friend. There are simply too many wonderful people around for my thesis-clouded mind to quickly come up with all the names.

Inger and Annica, what would we do without you? You've helped me navigate the intricacies of the university and the government bureaucracy, and done it with such warmth and good humor.

Kimmo... words do not seem sufficient to express how grateful I am to have had your love and support during all these years. Thank you.

Et les derniers mais non les moindres, un gros merci du fond du coeur à ma famille, Marie-France, Christian et Alexis, qui ont été des partisans infatiguables. Je vous aime fort.

Bibliography

[1] K. Nakamura *et al*. (Particle Data Group), *Review of particle physics*, *J. Phys*. **G37** (2010) 075021.

[2] B. Martin and G. Shaw, *Particle Physics*. John Wiley & Sons, Canada, 1997.

[3] R.K. Ellis, W.J. Stirling and B.R. Webber, *QCD and Collider Physics*, vol. 8 of *Cambridge Monographs on Particle Physics, Nuclear Physics and Cosmology*. Cambridge University Press, Cambridge, UK, 1996.

[4] M. Peskin and D. V. Schroeder, *An Introduction to Quantum Field Theory*. Harper Collins Publishers, New York, USA, 1995.

[5] T. Aaltonen *et al*. (CDF Collaboration), *Studying the Underlying Event in Drell-Yan and High Transverse Momentum Jet Production at the Tevatron*, *Phys. Rev.* **D82** (2010) 034001, [arXiv:1003.3146].

[6] ATLAS Collaboration, *Charged-particle multiplicities in pp interactions measured with the ATLAS detector at the LHC*, arXiv:1012.5104.

[7] T. Sjostrand, S. Mrenna, and P. Z. Skands, *PYTHIA 6.4 Physics and Manual*, *JHEP* **05** (2006) 026, [hep-ph/0603175].

[8] P. Z. Skands, *Tuning Monte Carlo Generators: The Perugia Tunes*, *Phys. Rev.* **D82** (2010) 074018, [arXiv:1005.3457].

[9] R. Barate *et al*. (LEP Working Group for Higgs boson searches), *Search for the standard model Higgs boson at LEP*, *Phys. Lett*. **B565** (2003) 61–75, [hep-ex/0306033].

[10] J. Alcaraz, *Precision Electroweak Measurements and Constraints on the Standard Model*, arXiv:0911.2604.

[11] TEVNHP Working Group, *Combined CDF and D0 Upper Limits on Standard Model Higgs-Boson Production with up to 6.7 fb^{-1} of Data*, FERMILAB-CONF-10-257-E, CDF Note 10241, D0 Note 6096 (2010).

[12] J. F. Gunion, S. Dawson, H. E. Haber, and G. L. Kane, *The Higgs hunter's guide*. Addison-Wesley, Menlo-Park, 1990.

[13] P. Binetruy, *Supersymmetry: Theory, experiment and cosmology*. Oxford University Press, Oxford, UK, 2006.

[14] K. Assamagan *et al*., *ATLAS Charged Higgs Boson Searches*, ATL-PHYS-INT-2008-046, ATL-COM-PHYS-2008-090 (2008).

[15] **ALEPH** Collaboration, A. Heister *et al*., *Search for charged Higgs bosons in e^+e^- collisions at energies up to $\sqrt{s}$ = 209-GeV*, *Phys. Lett.* **B543** (2002) 1–13, [hep-ex/0207054].

[16] T. Aaltonen *et al*. (CDF Collaboration), *Search for charged Higgs bosons in decays of top quarks in $p - \bar{p}$ collisions at $\sqrt{s} = 1.96$ TeV*, *Phys. Rev. Lett.* **103** (2009) 101803, [arXiv:0907.1269].

[17] V. Abazov *et al*. (D0 Collaboration), *Combination of $t\bar{t}$ cross section measurements and constraints on the mass of the top quark and its decays into charged higgs bosons*, *Phys. Rev. D* **80** (2009), no. 7 071102.

[18] V. Abazov, *et al*. (D0 Collaboration), *Search for charged Higgs bosons in top quark decays*, *Phys. Lett.* **B682** (2009) 278–286, [arXiv:0908.1811].

[19] J.D. Cockroft and E.T.S. Walton, *Experiments with High Velocity Positive Ions*, *Proceedings of the Royal Society of London. Series A, Containing Papers of a Mathematical and Physical Character* **129** (1930), no. 811 477–489.

[20] J.D. Cockroft and E.T.S. Walton, *Experiments with High Velocity Positive Ions. (I) Further Developments in the Method of Obtaining High Velocity Positive Ions*, *Proceedings of the Royal Society of London. Series A, Containing Papers of a Mathematical and Physical Character* **136** (1932), no. 830 619–630.

[21] Fermilab Visual Media Services, *Fermilab's Accelerator Chain*, 2000. http://www-visualmedia.fnal.gov/VMS_Site/gallery/stillphotos/2000/0600/00-0635D.hr.jpg.

[22] V. Abazov *et al*. (DØ Collaboration), *The Upgraded D0 Detector*, *Nucl. Instrum. Meth.* **A565** (2006) 463–537, [physics/0507191].

[23] DØ Upgrade Collaboration, *D0 silicon tracker technical design report*, DØ Note 2169 (1994).

[24] D. Adams *et al*., *The D0 Upgrade: Central Fiber Tracker, Technical Design Report*, DØ Note 4163 (1999).

[25] D. Adams, *Finding Tracks*, DØ Note 2958-2 (1998).

[26] H. Greenlee, *The D0 Kalman Track Fit*, DØ Note 4303 (2003).

[27] L. Groer for the DØ Collaboration, *DØ Calorimeter Upgrades For Tevatron Run II*, *Proceedings for the IXth International Conference on Calorimetry in Particle Physics* (2000).

[28] D. Denisov for the D0 Muon Group, *The DØ Experiment Muon System*, DØ Note 4440 (2004).

[29] B. Baldin *et al*., *Design of the Central Muon System*, DØ Note 3365 (1997).

[30] CERN, *LHC Yellow Book*, CERN-AC-95-05 (1995).

[31] C. Lefevre, *The CERN accelerator complex*, CERN-DI-060652 (2006). ©CERN.

[32] G. Aad *et al*. (ATLAS Collaboration), *The ATLAS Experiment at the CERN Large Hadron Collider*, *JINST* **3** (2008) S08003.

[33] ATLAS Collaboration, *ATLAS inner detector: Technical Design Report, 1 and 2*. Technical Design Report ATLAS. CERN, Geneva, 1997. CERN-LHCC-97-016, CERN-LHCC-97-017.

[34] J. Arguin *et al*., *Track Reconstruction Efficiency in 900 GeV Data*, ATL-COM-INDET-2010-010 (2010).

[35] G. Aad *et al*., *Track Reconstruction Efficiency in* $\sqrt{(s)}$*=7 TeV Data for Tracks with* $p_t > 100$ *MeV*, .

[36] ATLAS Collaboration, *ATLAS liquid-argon calorimeter: Technical Design Report*. Technical Design Report ATLAS. CERN, Geneva, 1996. CERN-LHCC-96-041.

[37] ATLAS Collaboration, *ATLAS tile calorimeter: Technical Design Report*. Technical Design Report ATLAS. CERN, Geneva, 1996. CERN-LHCC-96-042.

[38] ATLAS Collaboration, *ATLAS muon spectrometer: Technical Design Report*. Technical Design Report ATLAS. CERN, Geneva, 1997. CERN-LHCC-97-022.

[39] ATLAS Collaboration, *ATLAS level-1 trigger: Technical Design Report*. Technical Design Report ATLAS. CERN, Geneva, 1998. CERN-LHCC-98-014.

[40] P. Jenni, M. Nessi, M. Nordberg, and K. Smith, *ATLAS high-level trigger, data-acquisition and controls: Technical Design Report*. Technical Design Report ATLAS. CERN, Geneva, 2003. CERN-LHCC-2003-022.

[41] ATLAS Collaboration, *Performance of the Minimum Bias Trigger in p-p Collisions at Sqrt(s) = 900 GeV*, ATLAS-CONF-2010-025 (2010).

[42] P. Bechtle *et al*., *Identification of hadronic* τ *decays with ATLAS detector*, ATLAS-COM-PHYS-2007-066 (2007).

[43] E. F. Eisenhandler, *ATLAS Level-1 Calorimeter Trigger Algorithms*, ATL-DAQ-2004-011, CERN-ATL-DAQ-2004-011 (2004).

[44] V. Abazov *et al*. (DØ Collaboration), *A Precision Measurement of the Mass of the Top Quark*, *Nature* **429** (2005) 638.

[45] J. C. Estrada Vigil, *Maximal use of kinematic information for the extraction of the mass of the top quark in single-lepton t anti-t events at D0*, FERMILAB-THESIS-2001-07 (2001).

[46] M. F. Canelli, *Helicity of the W boson in single-lepton $t\bar{t}$ events*, FERMILAB-THESIS-2003-22 (2003).

[47] C. Garcia, *Precision Measurement of the Mass of the Top Quark in $p\bar{p}$ Collisions*, FERMILAB-THESIS-2007-21 (2007).

[48] MadWeight web page. http://cp3wks05.fynu.ucl.ac.be/twiki/bin/view/Software/MadWeight.

[49] LHCO data format. http://cp3wks05.fynu.ucl.ac.be/Manual/lhco.html.

[50] DØ Jet Energy Scale study group, *Jet Energy Scale at DØ RunII*, DØ Note 4720 (2005).

Acta Universitatis Upsaliensis

Digital Comprehensive Summaries of Uppsala Dissertations from the Faculty of Science and Technology 802

Editor: The Dean of the Faculty of Science and Technology

A doctoral dissertation from the Faculty of Science and Technology, Uppsala University, is usually a summary of a number of papers. A few copies of the complete dissertation are kept at major Swedish research libraries, while the summary alone is distributed internationally through the series Digital Comprehensive Summaries of Uppsala Dissertations from the Faculty of Science and Technology. (Prior to January, 2005, the series was published under the title "Comprehensive Summaries of Uppsala Dissertations from the Faculty of Science and Technology".)

Distribution: publications.uu.se
urn:nbn:se:uu:diva-142464

ACTA
UNIVERSITATIS
UPSALIENSIS
UPPSALA
2011